Mid-infrared absorptance of silicon hyperdoped with chalcogen via fs-laser irradiation

Meng-Ju Sher,[1] Yu-Ting Lin,[2] Mark T. Winkler,[1,a)] Eric Mazur,[1,2] Christian Pruner,[3] and Augustinus Asenbaum[3]
[1]*Department of Physics and Harvard University, 9 Oxford Street, Cambridge, Massachusetts 02138, USA*
[2]*School of Engineering and Applied Sciences, Harvard University, 9 Oxford Street, Cambridge, Massachusetts 02138, USA*
[3]*Department for Materials Research and Physics, University of Salzburg, Salzburg, Austria*

(Received 4 November 2012; accepted 22 January 2013; published online 14 February 2013)

Silicon hyperdoped with heavy chalcogen atoms via femtosecond-laser irradiation exhibits strong broadband, sub-bandgap light absorption. Understanding the origin of this absorption could enable applications for hyperdoped-silicon based optoelectronic devices. In this work, we measure absorption to wavelengths up to 14 μm using Fourier transform infrared spectroscopy and study sulfur-, selenium-, and tellurium-hyperdoped Si before and after annealing. We find that absorption in the samples extends to wavelengths as far as 6 μm. After annealing, the absorption spectrum exhibits features that are consistent with free-carrier absorption. Although the surface morphology influences the shape of the absorption curves, the data permit us to place an upper bound on the position of the chalcogen dopant energy levels. © *2013 American Institute of Physics*.
[http://dx.doi.org/10.1063/1.4790808]

I. INTRODUCTION

Pulsed laser processing creates novel materials with ultrahigh dopant concentration and tunable surface textures for enhanced light absorption.[1] Many studies focus on femtosecond laser (fs-laser) doping of silicon with heavy chalcogens (sulfur, selenium, or tellurium) because the material exhibits strong light absorption both above and below the bandgap of silicon, indicating a change in the electronic band structure.[2–4] The resulting material is called hyperdoped silicon because the dopant concentrations can be as high as 1 at. %, three orders of magnitude above the equilibrium solid solubility limit;[5–7] and at least 20% of the dopant atoms occupy substitutional sites.[8] Thermal annealing changes the chemical state of the dopant atoms and decreases sub-bandgap light absorption.[9,10] Although previous studies have shown that the sub-bandgap absorption extends down to at least 0.5 eV, a complete picture of the absorption mechanism remains unclear, as well as the influence of surface morphology and free-carrier absorption. Also, further investigation is necessary to understand the energy states introduced by the supersaturated dopants in silicon.

Chalcogen-doped silicon has been studied extensively for infrared (IR) detectors.[11,12] Photodetectors fabricated from S-hyperdoped Si have sub-bandgap photon responsivity to energies as low as 0.83 eV.[13] Furthermore, if sub-bandgap absorption in hyperdoped Si is due to the presence of an intermediate band, this material system could have applications in high-efficiency photovoltaics.[14] Evidence of intermediate band formation, such as metallic conduction, has been observed in other hyperdoped Si systems.[15,16] Therefore a better understanding of the energetics of the chalcogen dopants is important for further development of hyperdoped Si-based optoelectronic devices.

In this paper, we use mid-infrared absorption spectroscopy to study the dopant energy levels created in silicon hyperdoped with S, Se, or Te. IR spectroscopy yields information on transition probabilities between two energy states. Dilute chalcogen concentrations in silicon introduce occupied electronic states located between 100 and 300 meV below the conduction band edge,[17,18] and the energy levels of these states have been identified using IR absorption measurements.[19–21] At a concentration as high as 1 at. %, we expect the dopant energy levels to broaden into a band, and the absorption coefficient of an intermediate band formed by substitutional chalcogen atoms has been calculated using density-functional theory.[16,22] For Si doped with non-equilibrium concentrations of chalcogens, broad-band sub-bandgap absorption is commonly reported in the range of 0.5 to 1.2 eV (1.0–2.5 μm).[2–4,23,24] In this paper, we find that strong absorption in chalcogen-hyperdoped silicon extends to energies smaller than 0.4 eV and in some samples to 0.2 eV (3–6 μm); the shapes of the absorption curves are sensitive to the surface morphology of the samples. Additionally, upon annealing, sub-bandgap absorptance decreases, and in the case of Se- and Te-hyperdoping, a broad resonance feature emerges. Analysis of the absorption data results in bounds on the location of the chalcogen dopant energy levels in hyperdoped silicon, and we find that in addition to chalcogen dopants, free carriers also contribute to sub-bandgap absorption after annealing.

II. EXPERIMENTAL

Silicon wafers ((100) orientation, float zone grown, p-type, >3000 Ω cm) are cleaned to remove organic and metallic contaminants.[25] The wafer is placed in a vacuum

[a)]Present address: IBM T.J. Watson Research Center, 1101 Kitchawan Road, Yorktown Heights, New York 10598, USA.

chamber and irradiated at normal incidence with Ti:sapphire laser pulses with 80-fs pulse duration (center wavelength at 800 nm and 1-kHz repetition rate). For S doping, the vacuum chamber is filled with sulfur hexafluoride (SF_6) gas at a pressure of 6.67×10^4 Pa. For Se or Te doping the dopant precursor is a thermally evaporated 65-nm Se or Te film directly on the silicon wafer, and the vacuum chamber is filled with nitrogen buffer gas at a pressure of 6.67×10^4 Pa. The laser pulses have an average energy of 1.1 mJ and are focused to a spot size of 500 μm (FWHM of a Gaussian beam) to achieve a fluence of 4 kJ/m^2. A galvanometric scanning mirror system scans the laser beam across a 25×25 mm^2 area and translates subsequent pulses by 50 μm such that any given spot in the irradiated region is exposed to 80 laser pulses. Using the same parameters, we fabricated a control sample (Si:N_2) in the absence of chalcogen dopants using only nitrogen buffer gas. We fabricated an additional S-hyperdoped sample (Si:S-2) at a higher fluence (8 kJ/m^2 and 50 pulses) to achieve comparable microstructures and sub-bandgap absorptance as the Se- and Te-hyperdoped (Si:Se and Si:Te) samples.[26] After laser irradiation, samples are treated in one of three ways: unannealed, annealed at 730 K, or at 990 K. Annealing is performed for 30 min in a nitrogen environment.

We study the optical and electronic properties of these samples. We collect integrated transmission (T) and reflection (R) spectra and calculate absorptance ($A = 1 - R - T$). A UV-VIS-NIR spectrophotometer is used for visible and near-IR measurements (0.5–1.5 eV), and a Fourier transformed-infrared (FTIR) spectrometer is used for collecting mid-IR data (0.09–0.62 eV). Both the spectrophotometer and the FTIR spectrometer are equipped with integrating spheres in order to collect transmitted and reflected light at all angles. To study the electronic properties, we deposit 2-mm square Ti-Ni-Ag (20–20–200 nm, Ti adjacent to Si) contacts at four corners of the samples and perform resistivity and Hall measurements using the van der Pauw technique.[27]

III. RESULTS AND DISCUSSION

A. Upper bound on dopant energy levels

The near-IR and mid-IR absorptance of fs-laser hyperdoped samples before thermal treatment is shown in Figure 1; reflectance and transmittance data are presented as supplementary material.[28] For photons with energies greater than the bandgap of silicon, 1.1 eV, all samples exhibit enhanced photon absorption compared to the crystalline silicon substrate. Between 0.5 and 1.1 eV, all chalcogen-hyperdoped samples exhibit strong but featureless absorption. Below 0.5 eV, extended absorptance for chalcogen-hyperdoped Si decreases in the mid-infrared range, with the onset of a drop in absorptance varying with fabrication parameters.

As a comparison, at energies below the bandgap, the absorptance of a silicon substrate is approximately zero except at energies near the phonon vibrational modes (<0.18 eV). A sample irradiated with the absence of chalcogen dopant precursors, Si:N_2, exhibits sub-bandgap absorption only due to structural defects (Urbach states).[10,29,30] A recent study shows that absorption related to structural defects is reduced by annealing at a moderate temperature ($T \geq 575$ K), while

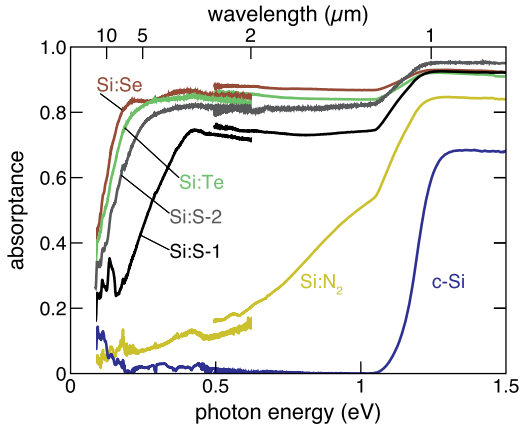

FIG. 1. Absorptance of chalcogen-hyperdoped silicon. Data for a control sample (Si:N_2) and the silicon substrate (c-Si) are also plotted for comparison. Data from 0.09 to 0.62 eV was collected using an FTIR spectrometer and data from 0.5 to 1.5 eV was collected using a UV-VIS-NIR spectrophotometer. The mismatch between the data from two instruments at 0.5 eV is about 3%.

chemical states or absorption related to the chalcogen dopants are minimally affected.[9,10]

Figure 2 shows scanning electron microscope (SEM) images of chalcogen-hyperdoped Si after fs-laser irradiation. The formation and structural characteristics of these samples have been discussed in detail in Ref. 26, and in this article we provide a brief summary of the difference in surface morphologies among the samples used in this study. First, Si:Se and Si:Te have similar surface morphologies. Under the same fabrication conditions, Si:S-1 has surface features that are smaller than Si:Se and Si:Te. At a higher laser fluence, Si:S-2 achieves similar feature size and comparable absorptance as Si:Se and Si:Te samples. By analyzing the SEM images, we obtain the average height (h) and spacing (w) of the surface features of these samples (Table I).

Sub-bandgap absorption of chalcogen dopants arises from optical excitation of an electron from a dopant energy level to the conduction band. Thus, a low-energy cutoff of the sub-bandgap absorption could represent the smallest energy required to optically excite an electron from a dopant energy level to the conduction band edge. In the following paragraph, however, we discuss the influence of surface morphology on the shape of the absorption curves of hyperdoped silicon. As a result, Figure 1 does not directly provide the location of the dopant energy level, although it does permit an estimation of the maximum energy difference between the level and the conduction band.

Surface morphology can increase the absorption of incident light by reducing reflection and/or increasing the optical path length inside the absorber. Figure 3(a) illustrates how the morphology contributes differently to anti-reflection and light trapping for different wavelengths of light. For wavelengths smaller than about twice the separation between conical spikes ($\lambda < 2w$), reflectance is reduced because incident light reflects multiple times in between the spikes, reducing the total amount of light reflected. The morphology also results in light trapping, because light enters the material at a non-normal angle, the total internal reflection angle of silicon in air is small, and the propagation path length is

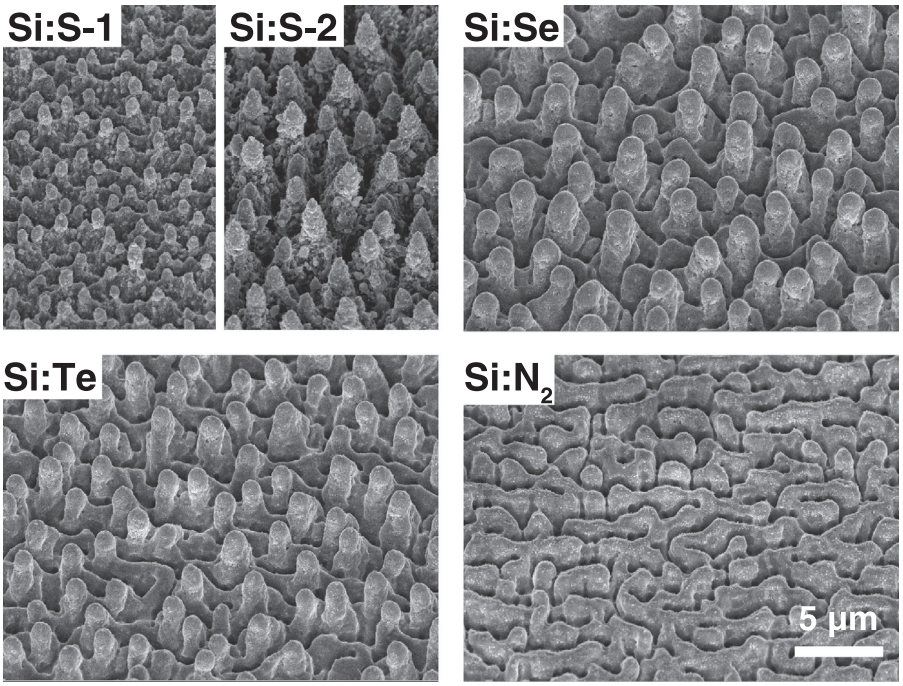

FIG. 2. Scanning electron micrographs of fs-laser hyperdoped silicon. The images are taken at a 45° angle to the surface. Si:S-1, Si:Se, Si:Te, and Si:N_2 are irradiated with the same fs-laser parameter: 4 kJ/m^2, 80 pulses. Si:S-2 is irradiated with 8 kJ/m^2, 50 pulses. After annealing, we examined all samples under SEM and observed no change in surface morphology in any of the samples.

extended.[1] For longer wavelengths ($\lambda > 2w$), the length scale of the surface features is smaller than the wavelength of light and the silicon and air form an effective medium. In this regime graded density is the main cause of low reflectance.[31] A graded density material does not change the direction of light propagation, so there is no light trapping. Graded density is only effective when the wavelength is smaller than 2.5 times the height of the surface roughness,[32] and at even longer wavelengths ($\lambda > 2.5h$), the surface appears optically smooth. Figure 3(a) illustrates how these surface features influence reflectance (due to anti-reflection) and transmittance (due to light trapping). Si:Se and Si:Te exhibit very similar surface morphologies: $w = 3.8\,\mu$m and $h = 4.6\,\mu$m (Table I). Figure 3(b) shows that the reflectance and transmittance curves of these two samples transition from high to low near wavelengths equal to $2.5h$ and $2w$, respectively. Although the transitions are not sharp, the transition wavelengths qualitatively agree with the analysis above. Similarly for Si:S-1 and Si:S-2, the transmittance and reflectance transition wavelengths qualitatively agree with the above analysis. Because the surface features are aperiodic, numerical simulation is challenging and we currently do not consider the quantitative details regarding changes in the optical path length and reflectivity as a function of wavelength, but this analysis shows that the infrared behavior is at least in part determined by the morphology of the surface.

TABLE I. Average surface feature spacing w and height h.

Sample	w (μm)	h (μm)
Si:S-1	2.3 ± 0.2	3.1 ± 0.5
Si:S-2	3.0 ± 0.3	5.4 ± 0.6
Si:Se	3.8 ± 0.5	4.6 ± 0.6
Si:Te	3.8 ± 0.5	4.5 ± 0.9
Si:N_2	0.9 ± 0.1	1.5 ± 0.5

The characteristics of sub-bandgap absorption depend on laser irradiation parameters, and it is illustrative to compare the absorptance curves of the two S-hyperdoped Si samples fabricated under different conditions. Si:S-2 (irradiated with higher laser fluence) has larger surface features (Figure 2) and the absorptance is higher overall than Si:S-1 (Figure 1). Furthermore, for Si:S-1 the broad band absorption extends to 0.42 eV and for Si:S-2 to 0.25 eV. Similar findings have been reported for different laser irradiation parameters in another S-hyperdoping study.[33] Previously we showed that the sulfur concentration in these two samples are comparable,[2] and hence the dopant-related absorption coefficients should be similar. Following our analysis of Figure 3, the difference in the surface morphology between Si:S-1 and Si:S-2 leads to differences in anti-reflection and light trapping, as evidenced by the variation in infrared behavior.

Thus, it is clear that the location of the absorption edge is influenced by surface roughness, and the absorption turn-offs in the mid-IR range shown in Figure 1 cannot be directly correlated to the energetics of the dopant atoms. However, because surface roughness can only serve to increase existing absorption mechanisms, the location of the turn-offs does place an upper bound on the energy gap between dopant energy levels and the conduction band edge, which is around 0.25, 0.20, and 0.21 eV for Si:S, Si:Se, and Si:Te, respectively.

B. Broad resonance features after annealing

Figure 4 shows mid-IR absorption spectra of each chalcogen-hyperdoped silicon sample before and after annealing. The above-bandgap absorptance (not shown) is unaffected by annealing[3] while sub-bandgap absorptance decreases with increasing annealing temperature. The reduction of sub-bandgap absorption agrees with earlier results we obtained, showing that the sub-bandgap absorption decreases smoothly with the diffusion length of dopant atoms.[10] For

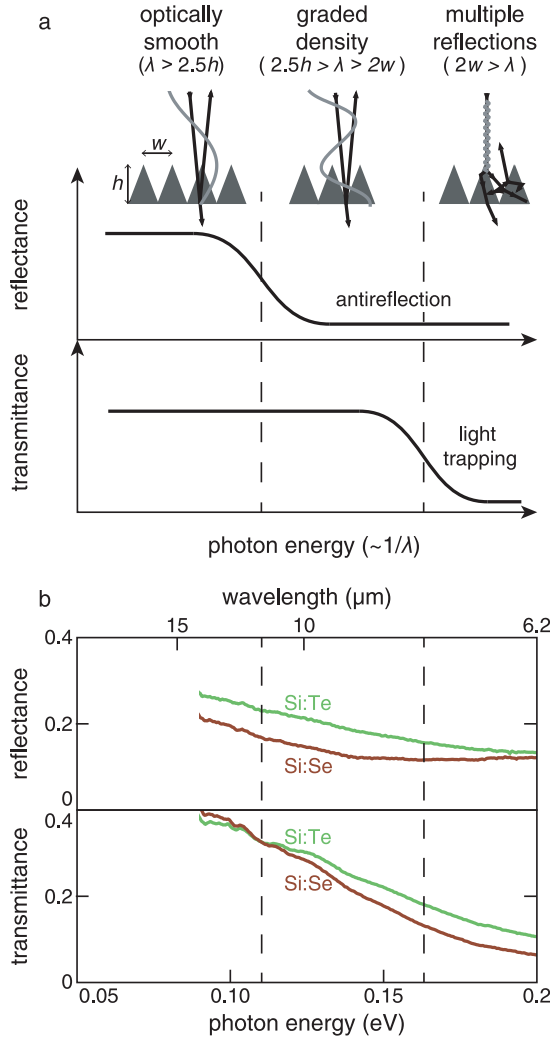

FIG. 3. (a) Illustration of light propagation though micrometer-scale structures with spacing w and height h, as well as the corresponding reflectance and transmittance as a function of photon energy (proportional to inverse wavelength). Three wavelength ranges represent different light and matter interactions: optically smooth (left), graded density (middle), and multiple reflections (right). The representative wavelengths are shown for the incoming light (gray); for each wavelength, three arrows indicate incoming, reflected, and transmitted light. (b) Reflectance and transmittance spectra of Si:Se (brown) and Si:Te (green) between 0.09 and 0.2 eV. The vertical dashed lines at 0.11 eV (11.3 μm) and 0.16 eV (7.6 μm) correspond to transition wavelengths at $2.5h$ and $2w$, respectively.

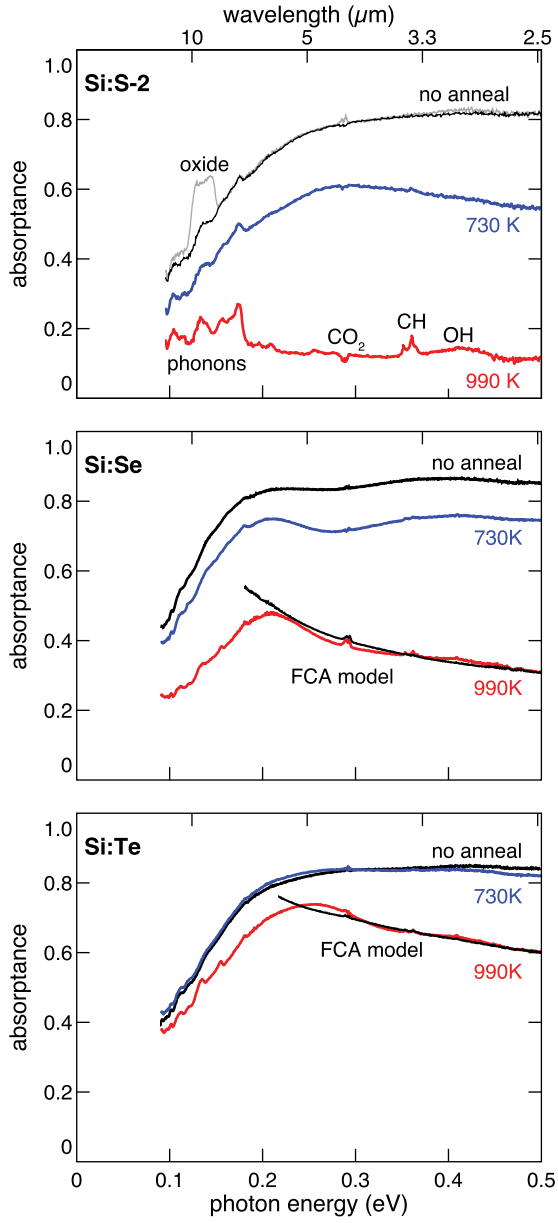

FIG. 4. Mid-infrared absorptance of Si:S-2, Si:Se, and Si:Te before (black) and after annealing at 730 K (blue) and 990 K (red). Except for the gray line, all Si:S-2 data are taken after a 5% HF etch for 1 min and the surface oxide absorption band from 0.13 to 0.15 eV is removed. Labels correspond to absorption features phonon vibrations and other contaminants: hydroxide (OH; centered at 0.42 eV),[44] hydrocarbon (CH; three peaks near 0.36 eV),[44] silicon phonons (below 0.13 eV and between 0.16–0.18 eV),[45] and CO_2 molecules in the spectrometer (0.29 eV).[46] The curves are fits of the free carrier absorption model in Eq. (2): $A(\varepsilon) = [1 - R(\varepsilon)](1 - ye^{-x/\varepsilon^2})$.

Si:Se, a resonance feature at 0.21 eV emerges after annealing at both 730 and 990 K, and for Si:Te a resonance signal emerges at 0.26 eV after annealing at 990 K. We also observe a broad maximum for Si:S-2 after annealing at 730 K, but after annealing at 990 K the sub-bandgap absorptance deactivates completely.

S-hyperdoped Si samples exhibit a broad oxide absorption band at 0.13–0.15 eV (gray line in Figure 4: Si:S-2), which can be removed with a dilute hydrofluoric acid (5% HF) etch. In addition, we identify features associated with phonon vibrations and other contaminants labeled in Figure 4. We do not observe—either before or after annealing—any absorption lines from dilute chalcogen dopants (ranging from 0.1 to 0.3 eV)[17,18] nor any absorption features related to sulfur compounds.[34] Due to the low signal below 0.09 eV, our measurement is not sensitive to absorption bands of possible precipitated compounds such as SiS_2, SiSe, $SiSe_2$, or Si_2Te_3.[35–37] Additional absorptance measurements at low temperature and at far-IR wavelengths could be useful for probing vibrational and electronic transitions with energies below 0.09 eV.[38–40]

After annealing, broad resonance signals emerge for chalcogen-hyperdoped silicon, and for the purpose of this discussion we focus on the Si:Se and Si:Te samples annealed at 990 K. The width of these resonances suggests that these local maxima are due to a combination of energy-dependent processes instead of a resonance transition between two energy states. For example, a broad maximum near the absorption

edge could emerge by combining these two effects: free-carrier absorption and light trapping. Free-carrier absorption increases with reducing photon energy, but reduced light trapping for energies below 0.16 eV ($\lambda < 2w$) decreases the overall absorption and thus results in a local maximum.

We fit the absorption curves at energies higher than the resonances as a combination of absorption due to free carriers and dopant atoms. The free-carrier absorption coefficient, α_{FCA}, is proportional to the carrier concentration, n, as well as the square of the wavelength, λ, ($\alpha_{FCA} \approx 2 \times 10^{-18}\lambda^2 n$, λ in units of μm and n in units of cm^{-3}).[41] Figure 4 shows fits to the data between 0.3 and 0.6 eV with an absorptance estimated from Beer's law,

$$A = (1 - R)(1 - e^{-(\alpha_{FCA} + \alpha_{dopant})dm}). \quad (1)$$

A and R are the measured absorptance and reflectance, respectively; d is the thickness of the hyperdoped layer which is enhanced by a factor of m due to light trapping; and α_{dopant} represents dopant-related light absorption that persists after annealing. In the range between 0.3–0.6 eV, we assume α_{dopant} is energy independent[16] and so is m from the light-matter interaction discussion above. We can then rewrite Eq. (1) as

$$\frac{A(\varepsilon)}{1 - R(\varepsilon)} = 1 - ye^{-x/\varepsilon^2}, \quad (2)$$

where ε is the photon energy, y and x are fitting parameters ($x = 3 \times 10^{-18} n_{sheet} m$, [eV^2]). The numerical fit yields $x = 0.04$; $y = 0.49$ for Si:Se, and $x = 0.04$; $y = 0.24$ for Si:Te.

The good fits between the data and model described above support our hypothesis that free carriers contribute to the shape of the absorption curves. We compare this fitting result with electronic measurements. Table II summarizes the electronic measurements of Si:Se and Si:Te after annealing at 990 K, and the measured majority carriers are electrons. Both Si:Se and Si:Te have similar sheet carrier concentrations suggesting the free-carrier absorption is similar for both samples, and we indeed obtain identical fit values of x for the two samples.

While the absorption and the electronic measurements qualitatively agree, the value for x calculated using sheet carrier concentration, n_{sheet}, in Table II is much smaller than the fitted value. Even with maximum light trapping ($m = 49$),[42] the measured carrier concentration is still two orders of magnitude too small to explain the absorption with free carriers only. This discrepancy could arise because the measured sheet carrier concentration is an average value of a non-uniform dopant distribution, and the situation is further complicated by the rough surface and non-uniform thickness of the hyperdoped layer.[26]

TABLE II. Hall-effect and resistivity measurements of Se- and Te-hyperdoped Si after annealing.

Sample	Annealing temperature (K)	Sheet resistance (kΩ)	Sheet carrier concentration (10^{12} cm^{-2})	Mobility (cm^2 V^{-1} s^{-1})
Substrate	…	146	0.11	380
Si:Se	990	2.2	−6.2	466
Si:Te	990	1.5	−6.0	692

In summary, in addition to broad band absorption due to dopant atoms, the low energy optical absorption displays the spectral dependence of free-carrier absorption (increasing with λ^2) for Si:Se and Si:Te annealed at high temperature. The combination of different wavelength-dependent processes, namely free-carrier absorption, which increases with wavelength, and light trapping, which decreases with wavelength, explains the observed broad resonance. The carrier concentration obtained from the electronic measurements, however, is too small to account for all the free-carrier absorption observed; we believe this discrepancy is due to the complications introduced by the rough surface. Methods for eliminating the surface roughness from fs-laser hyperdoping have recently been demonstrated,[43] offering a possibility to avoid absorption contributions arising from the surface morphology.

IV. CONCLUSION

We report mid-IR absorptance measurements of chalcogen-hyperdoped silicon, identify the influence of surface morphology on the absorptance curves, and place bounds on the location of the dopant energy levels. The surface morphology resulting from laser irradiation enhances anti-reflection and light trapping, and the low-energy cutoff of the mid-IR absorption is sensitive to the surface morphology. Our data place an upper bound on the energy difference between the dopant energy level and the conduction band of about 0.2 eV. After annealing, the sub-bandgap absorptance decreases and broad resonance features emerge that do not correspond to known defect absorption lines. We attribute the broad resonance features observed in Si:Se and Si:Te to competing wavelength-dependent processes, including free-carrier absorption and wavelength-dependent light trapping. Finally, we emphasize the importance of taking into account the effect of surface roughness when analyzing and comparing optical and electronic measurements.

ACKNOWLEDGMENTS

Several people contributed to this work. M.S. conceived of the experiment, fabricated the samples, and carried out electronic characterization. C.P. and A.A. carried out FTIR measurements. M.S., M.W., and Y.L. analyzed the data and prepared the manuscript. E.M. and A.A. supervised the research. The authors would like to acknowledge Benjamin Franta and Seungyeon Kang for their assistance in editing the manuscript. The research described in this paper was supported by The National Science Foundation under Contract Nos. CBET-0754227 and DMR-0934480. M.W. acknowledges the support from the NSF Graduate Research Fellowship program.

[1]M. J. Sher, M. T. Winkler, and E. Mazur, MRS Bull. **36**, 439 (2011).
[2]C. H. Crouch, J. E. Carey, M. Shen, E. Mazur, and F. Y. Genin, Appl. Phys. A: Mater. Sci. Process. **79**, 1635 (2004).
[3]M. A. Sheehy, B. R. Tull, C. M. Friend, and E. Mazur, Mater. Sci. Eng., B **137**, 289 (2007).

[4]C. Wu, C. H. Crouch, L. Zhao, J. E. Carey, R. Younkin, J. A. Levinson, E. Mazur, R. M. Farrell, P. Gothoskar, and A. Karger, Appl. Phys. Lett. **78**, 1850 (2001).
[5]R. O. Carlson, R. N. Hall, and E. M. Pell, J. Phys. Chem. Solids **8**, 81 (1959).
[6]H. R. Vydyanath, J. S. Lorenzo, and F. A. Kroger, J. Appl. Phys. **49**, 5928 (1978).
[7]E. Janzen, H. G. Grimmeiss, A. Lodding, and C. Deline, J. Appl. Phys. **53**, 7367 (1982).
[8]C. H. Crouch, J. E. Carey, J. M. Warrender, M. J. Aziz, E. Mazur, and F. Y. Genin, Appl. Phys. Lett. **84**, 1850 (2004).
[9]B. K. Newman, J. T. Sullivan, M. Winkler, M. J. Sher, M. A. Marcus, S. Fakra, M. J. Smith, S. Gradecak, E. Mazur, and T. Buonassisi, 24th European Photovoltaic Solar Energy Conference (Hamburg, Germany, 2009), p. 236.
[10]B. R. Tull, M. T. Winkler, and E. Mazur, Appl. Phys. A: Mater. Sci. Process. **96**, 327 (2009).
[11]N. Sclar, J. Appl. Phys. **52**, 5207 (1981).
[12]Y. A. Astrov, L. M. Portsel, A. N. Lodygin, V. B. Shuman, and N. V. Abrosimov, Infrared Phys. Technol. **52**, 25 (2009).
[13]J. E. Carey, C. H. Crouch, M. Y. Shen, and E. Mazur, Opt. Lett. **30**, 1773 (2005).
[14]A. Luque and A. Marti, Phys. Rev. Lett. **78**, 5014 (1997).
[15]M. T. Winkler, D. Recht, M.-J. Sher, A. J. Said, E. Mazur, and M. J. Aziz, Phys. Rev. Lett. **106**, 178701 (2011).
[16]E. Ertekin, M. T. Winkler, D. Recht, A. J. Said, M. J. Aziz, T. Buonassisi, and J. C. Grossman, Phys. Rev. Lett. **108**, 026401 (2012).
[17]E. Janzen, R. Stedman, G. Grossmann, and H. G. Grimmeiss, Phys. Rev. B **29**, 1907 (1984).
[18]H. G. Grimmeiss, E. Janzen, H. Ennen, O. Schirmer, J. Schneider, R. Worner, C. Holm, E. Sirtl, and P. Wagner, Phys. Rev. B **24**, 4571 (1981).
[19]N. S. Zhdanovich and Y. I. Kozlov, Sov. Phys. Semicond. (USSR) **10**, 1102 (1976).
[20]J. C. Swartz, D. H. Lemmon, and R. N. Thomas, Solid State Commun. **36**, 331 (1980).
[21]G. Grossmann, K. Bergman, and M. Kleverman, Physica B & C **146**, 30 (1987).
[22]K. Sánchez, I. Aguilera, P. Palacios, and P. Wahnón, Phys. Rev. B **82**, 165201 (2010).
[23]S. H. Pan, D. Recht, S. Charnvanichborikarn, J. S. Williams, and M. J. Aziz, Appl. Phys. Lett. **98**, 121913 (2011).
[24]I. Umezu, A. Kohno, J. M. Warrender, Y. Takatori, Y. Hirao, S. Nakagawa, A. Sugimura, S. Charnvanichborikarn, J. S. Williams, and M. J. Aziz, AIP Conf. Proc. **1399**, 51 (2011).
[25]*Handbook of Semiconuctor Wafer Cleaning Technology: Science, Technology and Applications*, edited by W. Kern (Noyes Publications, New Jersey, 1993).
[26]M. Smith, M. Winkler, M.-J. Sher, Y.-T. Lin, E. Mazur, and S. Gradečak, Appl. Phys. A: Mater. Sci. Process. **105**, 795 (2011).
[27]L. J. van der Pauw, Philips Tech. Rev. **20**, 220 (1958).
[28]See supplementary material at http://dx.doi.org/10.1063/1.4790808 for reflectance and transmittance data.
[29]A. Poruba, A. Fejfar, Z. Remes, J. Springer, M. Vanecek, J. Kocka, J. Meier, P. Torres, and A. Shah, J. Appl. Phys. **88**, 148 (2000).
[30]W. B. Jackson, N. M. Johnson, and D. K. Biegelsen, Appl. Phys. Lett. **43**, 195 (1983).
[31]Y. F. Huang, S. Chattopadhyay, Y. J. Jen, C. Y. Peng, T. A. Liu, Y. K. Hsu, C. L. Pan, H. C. Lo, C. H. Hsu, Y. H. Chang, C. S. Lee, K. H. Chen, and L. C. Chen, Nat. Nanotechnol. **2**, 770 (2007).
[32]P. B. Clapham and M. C. Hutley, Nature **244**, 281 (1973).
[33]Y. Liu, S. Liu, Y. Wang, G. Feng, J. Zhu, and L. Zhao, Laser Phys. **18**, 1148 (2008).
[34]S. Aldallal, M. Hammam, S. M. Alalawi, S. Aljishi, and A. Breitschwerdt, Philos. Mag. B **63**, 839 (1991).
[35]B. Begemann, J. Dorschner, T. Henning, and H. Mutschke, Astrophys. J. **464**, L195 (1996).
[36]S. Aldallal, S. Aliishi, M. Hammam, S. M. Alalawi, M. Stutzmann, S. Jin, T. Muschik, and R. Schwarz, J. Appl. Phys. **70**, 4926 (1991).
[37]K. E. Petersen, U. Birkholz, and D. Adler, Phys. Rev. B **8**, 1453 (1973).
[38]J. E. Griffiths, M. Malyj, G. P. Espinosa, and J. P. Remeika, Phys. Rev. B **30**, 6978 (1984).
[39]L. Andrews, P. Hassanzadeh, D. V. Lanzisera, and G. D. Brabson, J. Phys. Chem. **100**, 16667 (1996).
[40]A. Gaymann, H. P. Geserich, and H. v. Lohneysen, Phys. Rev. B **52**, 16486 (1995).
[41]D. K. Schroder, R. N. Thomas, and J. C. Swartz, IEEE Trans. Electron Devices **25**, 254 (1978).
[42]E. Yablonovitch, J. Opt. Soc. Am. **72**, 899 (1982).
[43]M. T. Winkler, M.-J. Sher, Y.-T. Lin, M. J. Smith, H. Zhang, S. GradeCak, and E. Mazur, J. Appl. Phys. **111**, 093511 (2012).
[44]P. R. L. Sarma, T. R. R. Mohan, S. Venkatachalam, V. P. Sundarsingh, and J. Singh, J. Mater. Sci. **27**, 4762 (1992).
[45]J. I. Pankove, *Optical Processes in Semiconductors* (Dover, New York, 1975).
[46]J. Susskind and J. E. Searl, J. Quant. Spectrosc. Radiat. Transf. **18**, 581 (1977).